Development of New ZrO_2-CaO-C Material for High Performance Anti-clogging Nozzle

Akinari SASAKI, Ling LI, Shigefumi MATSUMOTO, Katsumi MORIKAWA and Kiyoshi GOTO

Krosaki Harima Corporation
1-1 Higashihama-machi, Yahatanishi-ku, Kitakyushyu City 806-8586, Japan
Phone*: +81-93-622-7231SMS
Email*: Sasaki.fq4.akinari@krosaki.co.jp
(* : as representative)

ABSTRACT

In anti-clogging technologies for nozzles used in continuous casting of steel with the application of ZrO_2-CaO-C (ZCG) material, a prominent improvement was achieved by developing a novel ZCG material (notified as ZL1) which has not only unique persistent anti-clogging effects against alumina inclusion in molten steel but also excellent corrosion resistance with applying ZrO2-CaO raw materials containing a higher amount of CaO to prolong the anti-clogging performance of the conventional ZCG. Innovative materials group including the ZL1 registered the trade mark as EVERCLEAN™, have been expected to improve both productivity and quality of the products in the steel making process by using them as nozzles for the continuous casting system.

Keywords : Refractories for steel making process, Nozzles for continuous casting system, Molten steel flow, ZrO_2-CaO (ZC) raw material, ZrO_2-CaO-C (ZCG) material, Anti-clogging technology for nozzles

INTRODUCTION

Nozzles for continuous casting typified by two of upper nozzle and submerged entry nozzle (hereinafter SEN), are refractories utilized in the final process which has influences on the quality of the slab as product in the steel making process, so that high reliability and further high performance are required. Especially, clogging phenomenon due to adhesion of alumina inclusion seen in the inner bore of nozzles for continuous casting, the entrainment of bubbles and powder associated with the turbulent flow in the mold lead to decline in the quality of the slab, further since it may be forced nozzle exchange during casting, also cause a decrease in productivity. The prevention technology against such as alumina clogging has been approached on both sides of steel making operation and refractories application so far. Until now, the application of ZrO_2-CaO-C (hereinafter ZCG) material is a major countermeasure in the side of refractories, but since CaO content was limited to about 20 mass% at the highest due to the hydration reaction, a fully satisfied anti-clogging effect has not yet been obtained[1)]. In addition, as a method to improve the anti-adhesion property of the ZCG, although the formation of a calcium-silicate based phase by the addition of SiO_2 component utilizing the destabilization of ZrO_2 is thought to be somewhat effective[2)], there is a problem in the method that an excessive erosion of the ZCG might have occurred.

In this study, by using a high CaO content ZrO_2-CaO raw material, we have succeeded in developing a ZL1 as a novel ZCG material which contains more than 40mass% CaO, and we have commercialized it as a new EVERCLEAN™. This material has features that it forms enough amount of molten oxides layer at the interface with the molten steel, keeping the melt high viscous state with suspending the ZrO_2 in the molten oxides layer. These features make it possible to realize the new material that can maintain both anti-clogging and low erosion/corrosion characteristics to the end of casting process. The test results of the SEN applied the ZL1 material in the actual casting operation are also described in this report together with those of investigation on the change of molten steel components before and after the erosion/corrosion test[3)] by detecting the refractories derived inclusions in comparison with those of general purpose materials including conventional ZCG materials.

HIGH CaO CONTAINING ZrO_2-CaO RAW MATERIAL

According to the ZrO_2-CaO system phase diagram of Ruff et al.[4] a solid solution of free CaO and $CaZrO_3$ is formed when the CaO content exceeds 50 mol%. In other words, some CaO precipitates in a free form when the CaO content exceeds 32 mass%. The composition of the high CaO content ZrO_2-CaO raw material used in this study is shown in **Table 1**. Furthermore, the microstructure of the raw material with the elemental mapping image by EPMA is shown in **Figure 1**. **Table 2** shows the results of the spot analysis in the microstructure shown in **Figure 1**. The composition of the raw material itself indicates that the total CaO content is 46 mass%. In addition, in the spot analysis, (N1) with the light image consists of 33.8 mass% CaO and 65.7 mass% ZrO_2, which is confirmed to be close to the stoichiometry of the $CaZrO_3$. On the other hand, (N2) with dark image is 95 mass% CaO, confirming that it is free CaO. Furthermore, microstructure and elemental mapping image of the raw material show that the free CaO in the raw material precipitated as fine crystals of less than 10μm.

Table 1: Chemical composition of raw material

Composition / mass%	
ZrO_2	52.3
CaO	46.2
Others	1.5

Table 2: EPMA spot analysis for (N1) and (N2) in Figure 1

Spot analysis / mass%	(N1)	(N2)
ZrO_2	65.7	2.1
CaO	33.8	95.3
Others	0.5	2.6

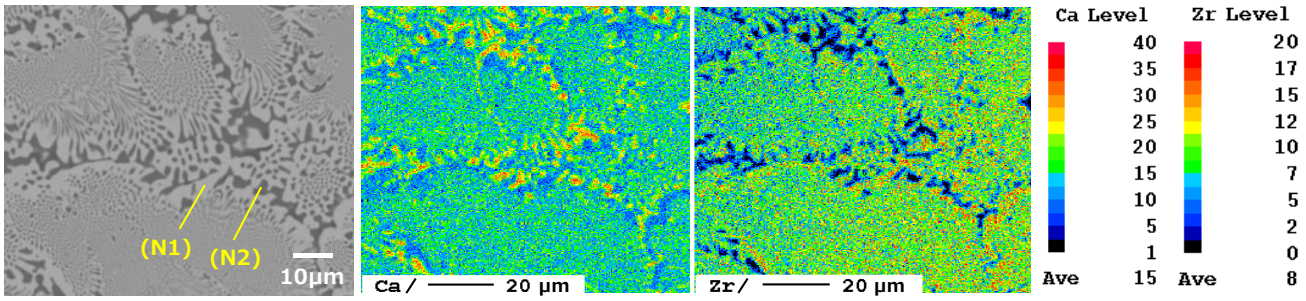

Figure 1. Elemental mapping image by EPMA for Ca and Zr of the raw material shown in Table 1.

DEVELOPMENT OF NOVEL ZCG MATERIAL

In order to compare the properties of the newly developed ZL1 material, with the other materials used for the SEN, those including one type of MgO-CaO system material and four types of general purpose material were prepared. The composition

Table 3: Composition and physical properties of each evaluated materials used for the SEN

		EVERCLEAN™		General purpose material			
		ZL1	ML1	ZCG	C-less	AG	ASG
Application way/position of SEN		Liner	Liner	Body or liner	Liner	Body or liner	Body
Composition / mass%	Free C	9	14	25	2	18	25
	ZrO_2	48	-	51	-	-	-
	CaO	42	42	16	1	-	-
	SiO_2	-	-	5	-	4	24
	Al_2O_3	-	-	-	72	77	45
	MgO	-	42	-	23	-	-
	Others	1	2	3	2	1	3
Apparent porosity / %		18.6	19.5	16.6	16.0	17.5	15.6
Modulus of rupture, *S* / MPa		3.9	2.1	11.9	4.0	6.9	7.7
Elastic modulus, *E* / GPa		4.0	3.0	14.1	15.5	7.0	7.8
Thermal expansion at 1000℃, *α* / %		0.37	0.30	0.48	0.60	0.33	0.23
Thermal shock resistance; *S* / (*E*·*α*)		264	233	176	43	299	429

and representative physical properties of these materials and the ZL1 are summarized in **Table 3** together with the application way/position to the SEN. ML1, MgO-CaO-graphite material has been commercialized together with the ZL1 as trade mark of EVERCLEAN™ applied to the liner of the SEN as anti-clogging material. Further, conventional ZCG and carbon-less material (hereinafter C-less) are used generally as an anti-clogging material in the steel industries, Al_2O_3-graphite (hereinafter AG) is used for nozzle body or liner material with specification of the intensified corrosion resistivity, Al_2O_3-SiO_2-graphite (hereinafter ASG) is used for nozzle body material with specification of the intensified thermal shock resistivity. [5), 6)]. The newly developed ZL1 has high CaO content compared with the conventional ZCG, and since it is designed to a lower carbon content, it is characterized by having both specifications of the anti-clogging and the erosion/corrosion resistance. It also features a lower thermal expansion coefficient than the conventional ZCG and C-less, and thus has an excellent thermal shock fracture resistance coefficient ($R=S(1-v)/(E \cdot \alpha)$, where S: modulus of rupture, E: elastic modulus, v: Poisson's ratio, α: thermal expansion rate at 1000 °C, we ignore the influence of Poisson's ratio here.). Generally, a material containing a large amount of CaO like EVERCLEAN™ is basic and known to exhibit a high thermal expansion, nevertheless, the ZL1 and the ML1 both included in the EVERCLEAN™ have not necessarily high thermal expansion compared with the other general purpose materials such as ZCG and C-less as shown in **Table 3**. The reason is that these materials are designated to compose of the phase with different characteristics which can compensate own weak point each other, more concretely in this case, that is a designated formation of the porous zone around the surface of the coarse oxide aggregate in the microstructure in terms of a special treatment in the powder processing of the material. On the heating of such material, since the occurred large expansion in the coarse oxide aggregates is absorbed nicely into the porous zone surrounding them, thus the thermal expansion of the material itself becomes not so large. Using the technique[7), 8)] which was developed originally as the combination of the materials for the continuous casting nozzle to endure the thermal shock, we can produce the basic materials with relatively low thermal expansion.

CHARACTERIZATION OF NOVEL ZCG MATERIAL

Alumina adhesion test in laboratory was conducted to compare the degree of surface damages in the tested refractories after the test in order to confirm the superiority of the newly developed ZL1 material. In addition to the test, the investigation on the change in the molten steel component including the inclusions before and after the test was also carried out in order to confirm the effect of species of the refractories used as the nozzle on the composition of the steel processed by the nozzle. Details of these contents are described below.

Alumina Adhesion and Erosion

Assuming the damages suffered the refractories applied in the inner wall of the nozzle, their alumina adhesion characteristics were investigated by the erosion/corrosion test in which four specimens of the refractories are rotated in the Al-killed molten steel at high speed of 200rpm simulating the flow of molten steel in the nozzle. The rotation of the specimens makes suspend the inclusions in the molten steel by the stirring action and to accelerate the reaction at the hot surface of the specimens with the molten steel under the flow. **Figure 2** shows a schematic illustration of the test apparatus. About 10 kg of low-carbon steel

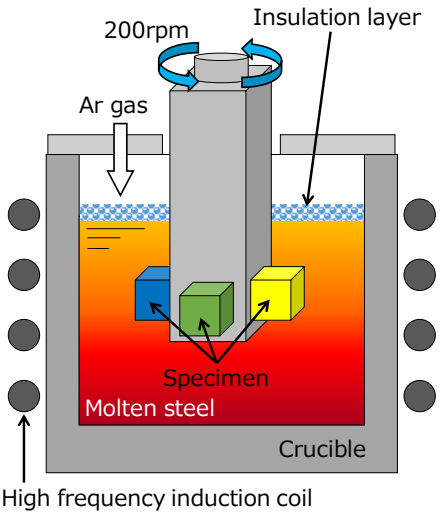

Figure 2. Schematic illustration of erosion/ corrosion test apparatus and test set-up.

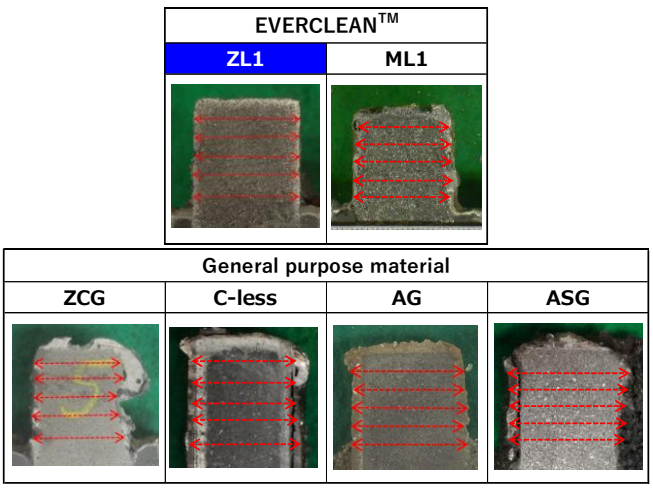

Figure 3. Cross section view of each specimen after erosion/corrosion test resulting in both erosion for ZL1, ML1 and ZCG and adhesion for C-less, AG and ASG.

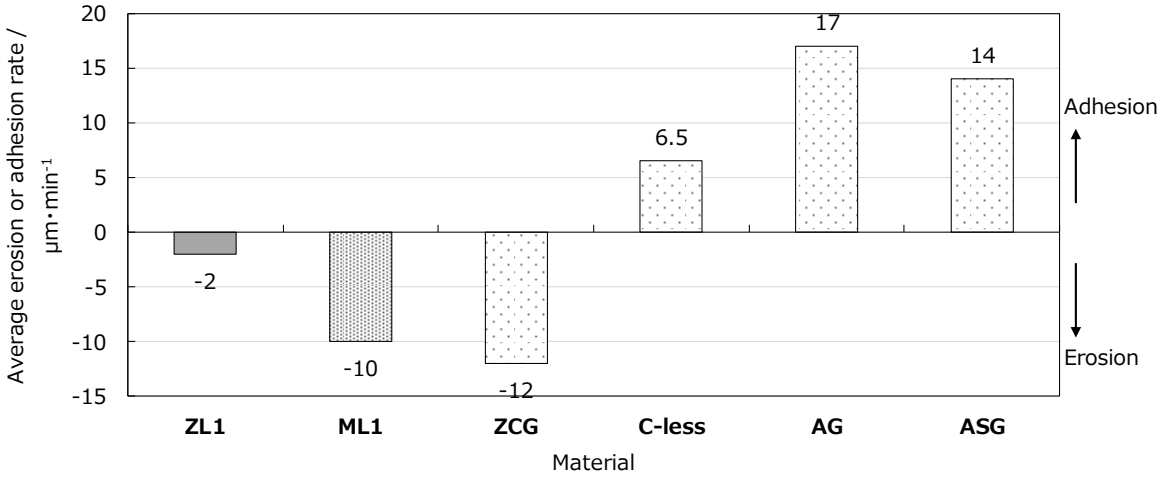

Figure 4. Comparison of measured erosion or adhesion rates in the erosion/corrosion test for each specimen.

was melted in a crucible heated by a high frequency induction furnace at 1550℃, and as deoxidizing agent to the molten steel, metallic Al of 0.2kg was added into the molten steel which corresponds to 0.2 mass% by the external multiplication. A refractory stirring rod attached the specimens (in size of 20×20×30mm) in the tip was immersed in the crucible and rotated continuously at 200 rpm for 120min. The average alumina deposition rate or erosion rate of each specimen was calculated from the dimensional changes before and after the test. **Figures 3** and **4** show the comparison of the cross section view of each specimen after the test and the average adhesion rates determined by the test, respectively. As shown in the figure, the ML1 eroded considerably and the conventional ZCG eroded more severely. The erosion rate of the newly developed ZL1 was as low as about 1/6 of the conventional ZCG. On the other hand, all of the other four general-purpose materials showed adhesion, where the C-less had the lowest rate, and the order was C-less < ASG < AG. As described above, the ZL1 material exhibited the highest adhesion resistance property.

Molten Steel Composition before and after the Erosion/Corrosion Test

Using the same materials for the crucible and stirring rod contacting with the molten steel, the emergence of the refractories-derived components due to the test specimens in the molten steel after the erosion/corrosion test was carefully checked. Similarly to the method shown in **Figure 2**, the erosion/corrosion test was carried out with only difference of the amount of the metallic Al to be added as a deoxidizer in total 0.5 mass% (0.5kg) by external multiplication with respect to the molten steel weight. The molten steel samples collected after the test were subjected to analyze the chemical composition precisely. In the previous studies[9), 10)], it was presumed that the alumina adhesion occurring on the refractories hot surface was caused by the chemical reactions shown in Eqs. (1) to (3).

$$SiO_2\,(s) + C\,(s) = SiO\,(g) + CO\,(g) \quad \text{..... (1)}$$

$$SiO\,(g) + 2/3\,[Al] = 1/3Al_2O_3(s) + [Si] \quad \text{..... (2)}$$

$$CO\,(g) + 2/3\,[Al] = 1/3Al_2O_3\,(s) + [C] \quad \text{..... (3)}$$

That is, gas components such as SiO and CO formed by the reaction inside the refractories diffuse to the interface with the molten steel, and oxidize Al retained in the molten steel, with depositing alumina as adhesion layer on the refractories. Further, since these gases pass through the alumina adhesion layer, the deposition of alumina can be grown. At the same time, the gaseous components of SiO and CO diffused into the molten steel will be picked up as carbon (hereinafter C) and silicon (hereinafter Si). Thus, the C pick-up in the steel is considered to be realized. Therefore, as an index of the molten steel contamination, the amounts of C pick-up for each material measured after the test were subtracted from the initial amount of the C in the steel. The results of the subtraction for each material are shown as the change in C concentration and compared each other in **Figure 5**. The C concentration increased in the ML1 as an anti-clogging material and the general-purpose materials ZCG, AG and ASG, because of the C leaching into the molten steel due to erosion during test for the ML1 and ZCG materials, and by the absorption of refractories-derived C into the molten steel through the chemical reactions of the Eqs. (1) and (3). The increase in the C concentration in the molten steel, thus becomes a second indication of the alumina deposit on the refractories hot surface.

In contrast to the above four materials, the materials of the newly developed ZL1 and the C-less, showed extremely lower amount of the C pick-up, resulting in a negative shift of the C concentration change. It occurred probably by vaporizing the C

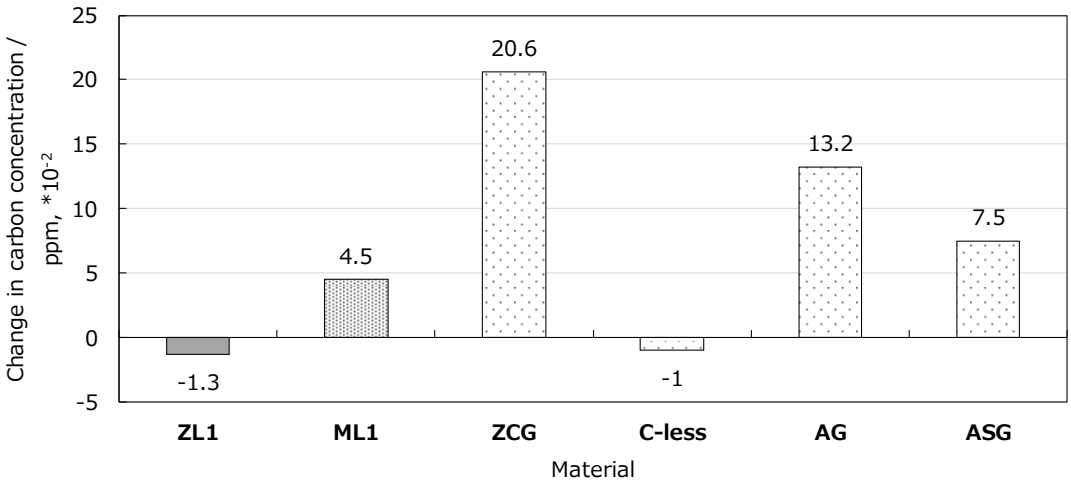

Figure 5. Change of carbon concentration in molten steel before and after the erosion/corrosion test.

somewhat in the molten steel during the test due to difficulty of complete sealing of the apparatus. Since all the materials were tested under the same condition, the amount of the C pick-up must be quite small for the ZL1 and the C-less compared with the others four materials, and comparison of the results among the materials tested is meaningful. The elution of the refractories-derived components into the molten steel can be suppressed by using the ZL1 and the C-less materials as nozzle even in the actual operation as well. The amounts of the C pick-up are considered to be almost equivalent for the ZL1 and the C-less materials even though they have differences in the contents of the free carbon 9 to 2 mass% and the reactions with the molten steel at the hot surface in forming to unforming the molten oxides layer. According to the results obtained, the newly developed material ZL1 has a quite favorable feature for the refractories to confine the molten steel contamination within extremely low levels when it is used as the SEN in the continuous casting system.

Hot Surface after the Erosion/Corrosion Test

Figure 6 shows the results of SEM observation and EPMA elemental mapping of the hot surface for the ZL1 and the conventional ZCG after the erosion/corrosion test. **Table 4** shows the results of surface analysis and the calculated amount of liquid phase using FactSage™ 8.1 for the squared areas (A1) to (B3) in the SEM images shown in **Figure 6**. In the ZL1, a continuous dense layer with a thickness of about 1 mm is formed on the hot surface, and in the area of (A1) the CaO content is 37.8 mass%, which is higher than that of the conventional ZCG. In addition, 92.7% liquid phase at 1550℃ calculated by the FactSage™ 8.1 indicates the existence of a liquid CaO rich Al_2O_3-CaO-ZrO_2 molten oxides layer on the hot surface of the ZL1. Furthermore, according to the analysis of the (A2), the CaO content in the slightly apart from the hot surface is as high as 52

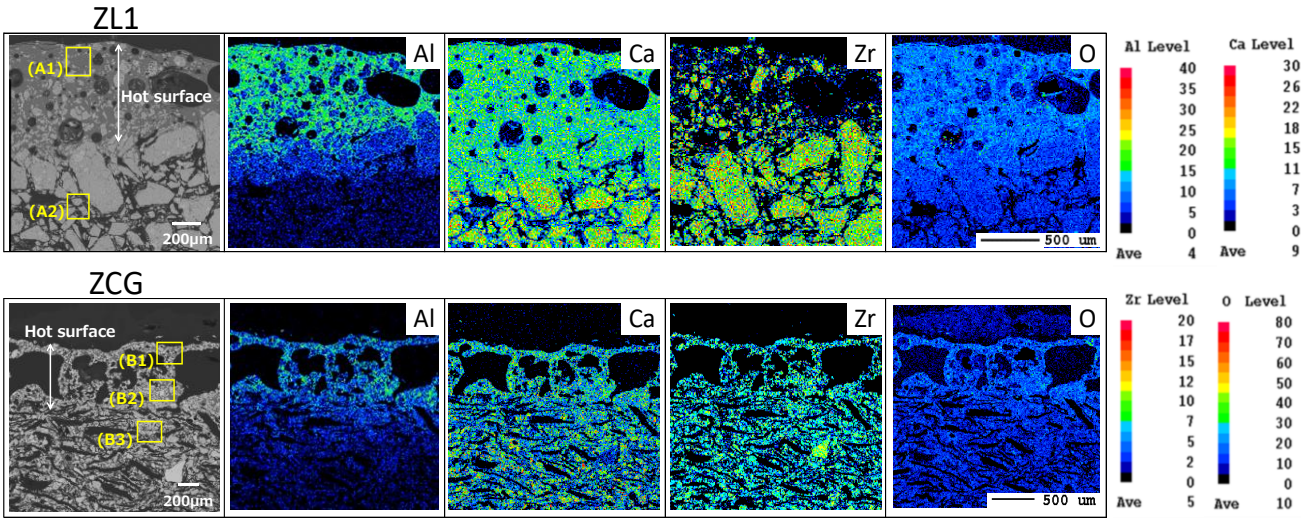

Figure 6. SEM microstructure and EPMA elemental mapping of hot surface for ZL1 and conventional ZCG.

Table 4: Composition of the oxide component in each area determined by EPMA surface analysis and calculated amount of liquid phase ratio at 1550℃ using the FactSage™ 8.1

Material		ZL1		ZCG		
Squared area in Figure 6		(A1)	(A2)	(B1)	(B2)	(B3)
Oxide component / mass%	Al_2O_3	46.1	3.9	33.1	29.0	13.6
	SiO_2	0.2	1.3	0.0	0.4	7.2
	CaO	37.8	52.1	22.0	21.2	26.1
	FeO	0.2	0.0	0.4	0.1	0.3
	ZrO_2	15.2	41.8	44.4	49.5	53.0
Liquid phase ratio at 1550℃ / mass%		92.7	12.3	8.6	19.9	4.7

mass%, which seems to source of the CaO to be supplied continuously to the interface with the molten steel from inside of the material, in the amount sufficient to inhibit from the alumina deposit on the hot surface.

On the other hand, in the conventional ZCG, a porous layer with about 0.5mm thickness containing large bubbles is observed at the interface with the molten steel, and for the areas (B1) and (B2) the results of analysis indicate that ZrO_2 is about 44 to 50 mass% and CaO is about 21 to 22 mass%, and a liquid phase ratio is lower than 20%, and a phase with high ZrO_2 with the lowered CaO is formed. The observed porous reaction layer may easily dissolve into the molten steel, presuming to increase both in the erosion rate and the amount of C pick-up, compared with the ZL1.

The microstructures with the higher magnification are shown in **Figure 7**, and the results of the spot analysis for (a1) to (b3) in the both micrographs are shown in **Table 5**. In the ZL1, the results of the spot analysis indicate that the spot (a1) is Al_2O_3-CaO-ZrO_2 molten oxides formed by the reaction of the free CaO in the ZrO_2-CaO raw material with alumina in the molten steel, and the spot (a2) is $CaZrO_3$ from the composition closely resembled to (N1) shown in the Table 2. The compound $CaZrO_3$ suspended in the molten oxides (a1) existing as the small particulates in size of less than 10μm and their agglomerates in size of about 100μm, is transferred to the hot surface to supply the CaO continuously for inhibiting the alumina deposition. In the conventional ZCG, some fine particles are also observed in **Figure 7**, but according to the spot analysis of (b2) and (b3) corresponding to these particles, their compositions are almost close to that of the CaO-stabilized ZrO_2. Thus, the molten oxides layer formed on the hot surface of the conventional ZCG is porous, and the liquid phase (b1) ratio is much lower than that of the (a1) and the particulates of ZrO_2 containing CaO is larger than the CaZrO3 (a2) make difficult to supply the CaO to the hot surface enough amount to inhibit the alumina deposition.

Michelic and Bernhard[11] have summarized the proposed materials for anti-clogging layers in the SEN as the results of literature survey in their review paper published recently, and have indicated that reaction of CaO in refractories with alumina inclusions to form an oxide phase with low melting point and high wettability is resulting in a decrease of the attractive force and the prevention of alumina deposits. When the CaO became depleted in the refractories, however, the favorable effect of anti-clogging action is expired. Although the problem was that the termination of the effect tends to come relatively earlier, the present material we developed ZL1 can solve the problem by prolonging largely the effective duration of anti-clogging as described previously.

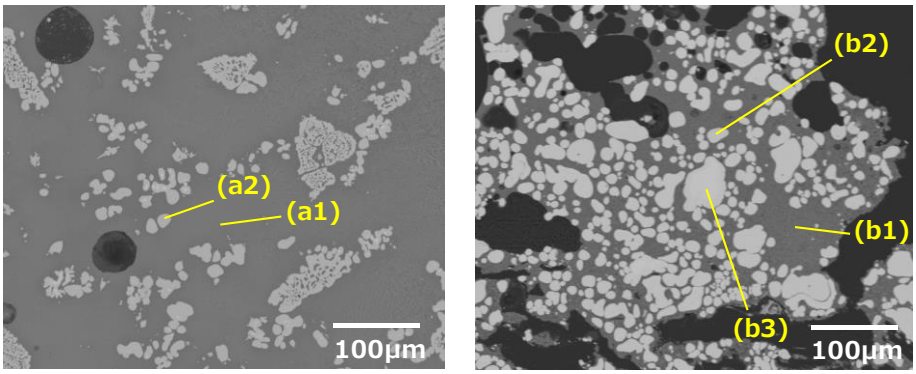

Figure 7. SEM microstructure and position of spot analysis by EPMA for ZL1 (a) and conventional ZCG (b).

Table 5: Composition of the oxide component determined by EPMA spot analysis and calculated amount of liquid phase ratio at 1550℃ using the FactSage™ 8.1

Material		ZL1		ZCG		
Spot in Figure 7		(a1)	(a2)	(b1)	(b2)	(b3)
Oxide component / mass%	Al_2O_3	53.0	0.4	54.0	0.3	0.2
	SiO_2	0.0	0.0	1.3	0.0	0.0
	CaO	31.2	33.2	30.3	10.9	3.4
	FeO	0.2	0.2	0.0	0.1	0.2
	ZrO_2	15.6	66.2	11.9	88.2	95.8
Liquid phase ratio at 1550℃ / mass%		95.7	1.6	97.0	0.0	0.0

Automatic Inclusion Analyzer to detect Refractories-derived Inclusions

In order to investigate the emergence of the inclusions in molten steel contacted with the refractories, the molten steel sample after the previously described erosion/corrosion test for the ZL1 material was subjected to the MQA (metal quality analyzer). **Figure 8** shows the particle size distribution of inclusions composed mainly of Zr considered to be derived from the ZL1. The fine inclusions of 10μm or less are detected by the analyzer. Further, **Figure 9** shows three types of the images of the detected inclusions mainly composed of Zr together with analyzed composition of them and value of DMAX. The DMAX is the maximum particle size of this inclusion, and their values of the DMAX were less than 10μm. Such size of particles must be too small to detect by the MQA as the detrimental inclusions for the steel products.

On the other hand, the emergence of the inclusions in the molten steel for the case of the ML1 material was also investigated in the same way. **Figure 10** shows the particle size distribution of the inclusions mainly composed of Mg considered to be derived from the ML1, and **Figure 11** shows the three types of images of the detected inclusions mainly composed of Mg. Inclusions with the DMAX values higher than 20μm was detected in the molten steel sample after the erosion/corrosion test with the ML1. The size of inclusions in the case of the ML1 was apparently larger than the ZL1 by comparing the **Figures 8** and **9** with the **Figures 10** and **11**.

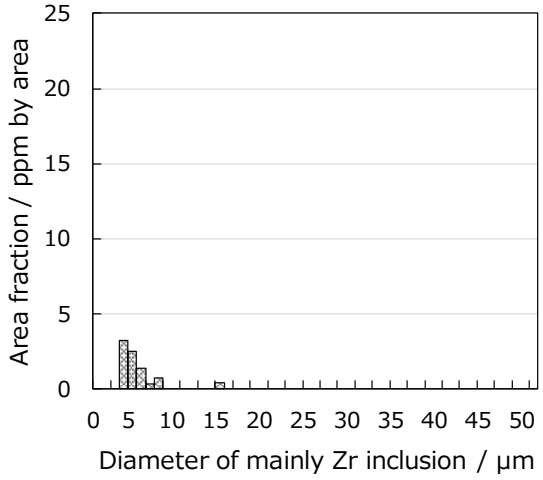

Figure 8. Particle size distribution of Zr inclusions in the molten steel after the erosion/corrosion test for ZL1 material.

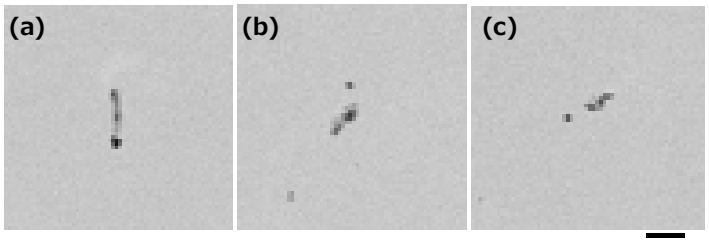

	Composition / mass %					DMAX / μm
	Zr	Al	O	C	N	
(a)	35	16	-	15	22	9.2
(b)	40	24	28	-	4	7.4
(c)	33	24	29	-	11	7.0

Figure 9. Appearance and analyzed composition for detected inclusions with relatively large particle size mainly composed of Zr and their DMAX values after the erosion/corrosion test for ZL1 material.

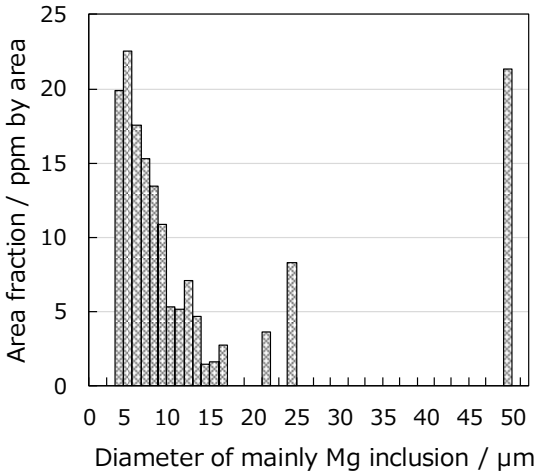

Figure 10. Particle size distribution of Mg inclusions in the molten steel after the erosion/corrosion test for ML1 material.

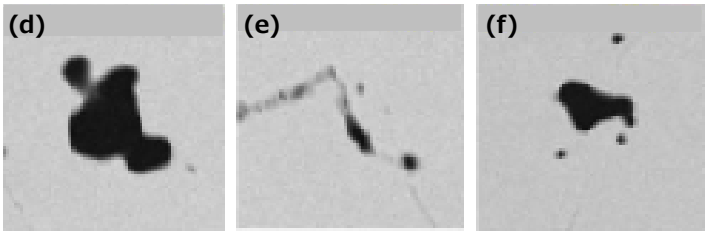

	Composition / mass %					DMAX / μm
	Mg	Al	Ca	O	C	
(d)	45	0	2	52	1	22.0
(e)	38	0	0	57	2	14.0
(f)	46	0	0	58	0	12.0

Figure 11. Appearance and analyzed composition for detected inclusions with relatively large particle size mainly composed of Mg and their DMAX values after the erosion/corrosion test for ML1 material.

STRUCTURAL EVALUATION OF EVERCLEAN™ APPLIED THE ZL1

We produced EVERCLEAN™ which applied the anti-clogging material ZL1 having the above-mentioned features to the inner wall of SEN, and tested the performance as the nozzle using a pouring test method [12] simulating the thermal history in the early stage of actual casting operation. **Figures 12** and **13** show schematic illustrations of the longitudinal cross cut view of the SEN and the pouring test apparatus, respectively. The SEN produced here was made of the structural materials in which the ZL1 was applied to the inner wall part, and the common general purpose materials AG and the ZCG to the main body and the ZG to the powder line. The apparatus used here was originally designed and devised by author et a1.[12] to evaluate the durability of ladle shroud against pouring of the molten pig iron into the inner bore of the shroud without preheating, for certain duration

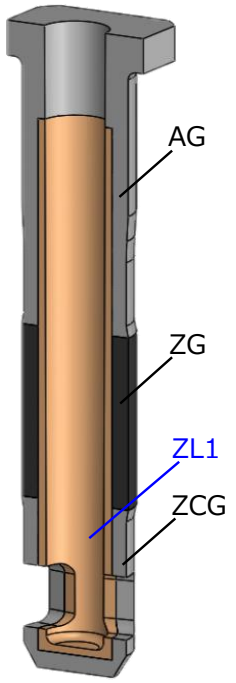

Figure 12. Half-cut illustration of the SEN image for pouring test.

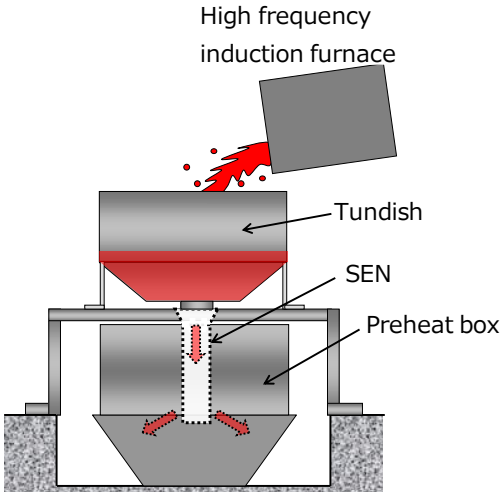

Figure 13. Schematic illustration of molten metal pouring test.

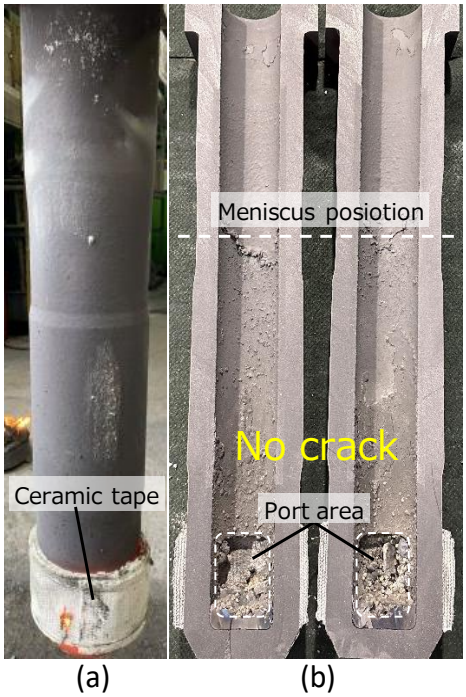

Figure 14. Appearance (a) and cross section (b) of SEN after pouring test.

of time by checking afterward the degree of cracking due to the thermal shock. In the present test, the 2 ton of pig iron which was heated and molten at 1650-1700℃ in the high frequency induction melting furnace, was poured into the SEN which was preheated at about 500℃ in the nozzle inner bore side, through the tundish at temperature about 1600℃.

Under the test condition of the limited amount of the molten pig iron to be poured in one charge, since the outlet port drawn in **Figure 12** at the near bottom side of the SEN, is too large to reserve somewhat molten pig iron, the port was closed both sides by lapping the ceramic tape around the lower position of the SEN as shown in Figure 14 (a) and (b), with remaining a small discharging hole of 10mm diameter bored on the ceramic tape. Using the SEN pretreated as mentioned above, the pouring test could be implemented to heat-up the nozzle enough to suffer the thermal shock by filling the whole part of the SEN with the molten pig iron. The results of the test is shown in **Figure 14** (a) and (b) as the outer appearance and the sliced cross section of the SEN into halves lengthwise, respectively after the pouring test. No flaws such as crack were found in the nozzle after the test, indicating the effectiveness of the SEN as a structural body to which the ZL1 was applied.

RESULTS OF ACTUAL CASTING OPERATION

Casting tests of the SEN applied the EVERCLEAN™ to the liner were conducted in the actual production line to evaluate the anti-adhesion and erosion properties of the ZL1 and the conventional ZCG, at the same time by using the immersion nozzle with the inner wall surface arranged specially as shown in **Figure 15**. The result of the test is shown in **Figure 16** after 6 heats casting of low carbon steel, as the picture of cross section in the longitudinal centerline of the nozzle closing up the section including the both positions of the liner materials of the ZCG and the ZL1. As apparently shown in the picture, the nozzle inner bore lined by the ZCG has thick layer of the alumina deposit, whereas the bore lined by the ZL1 is kept clean without deposit in spite of the observed slight traces of erosion.

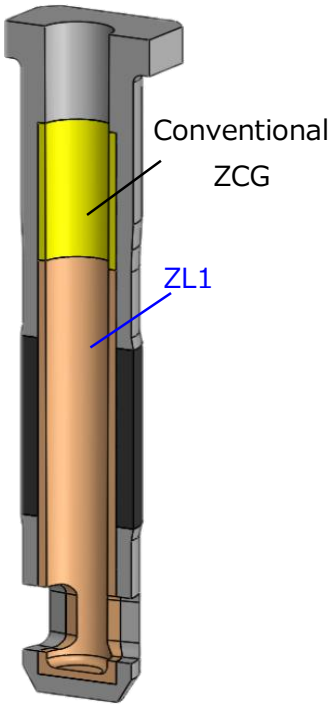

Figure 15. Half-cut illustration of the SEN image for using actual casting test.

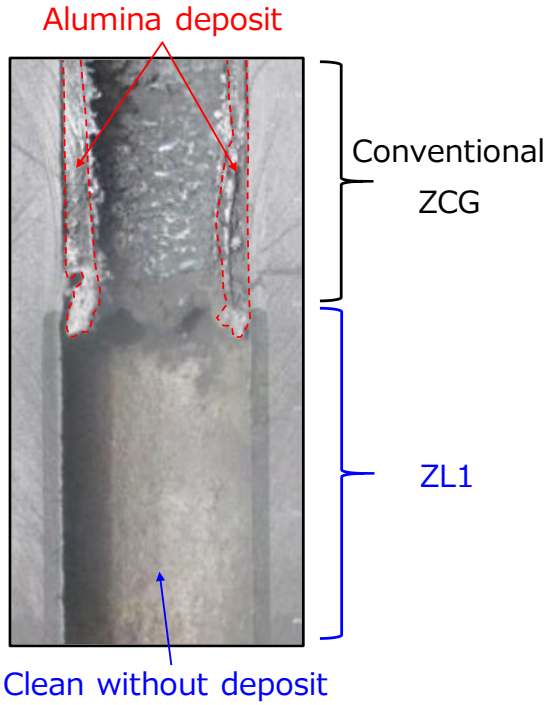

Figure 16. Cross section of the SEN after 6 heats of the low carbon steel in the actual casting test.

APPLICATION AND ARRANGEMENT OF THE DEVELOPED MATERIALS TO THE FIVE TYPES OF SEN

As the material for the main body of the SEN, we have also developed ZB1 as the group of EVERCLEAN™. The chemical composition and physical properties of the ZB1 are shown in **Table 6**. The exemplary design of five types of SEN to which ZL1 and ZB1 are applied as shown in **Figure 17**. Mizobe et al.[13), 14), 15), 16)] made many efforts to optimize the shape of both tundish upper nozzle and the port of SEN based on the principle of the energy minimum in the molten steel flow. They have succeeded to stabilize the flow by using nozzle with a novel shape derived from their theory. The shape derived was a biquadratic curve in the profile different from the original shape with the straight lines. In the SEN, their efforts resulted in the shapes I and II different from the general shape and a type for thin slab casting in Figure 17. The materials ZL1 and ZB1 are applied to all the five types of the SEN including those for thin slab casting. Such an application of superior materials like the ZL1 and ZB1 to the shape optimized nozzles makes a remarkable improvement on the steel making process in both productivity and quality. Actually, a stable molten steel flow continues to the end of the casting operation as long as the initial shape of the nozzle is maintained.

Table 6: Composition and physical properties of ZB1

		EVERCLEAN™
Material		**ZB1**
Application way/position of SEN		Body
Composition / mass%	Free C	20
	ZrO_2	40
	CaO	39
	Others	1
Apparent porosity / %		15.9
Modulus of rupture, *S* / MPa		6.5
Elastic modulus, *E* / GPa		5.0
Thermal expansion at 1000℃, *α* / %		0.30
Thermal shock resistance; *S* / (*E*·*α*)		433
Average erosion or adhesion rate / μm·min^{-1}		-7

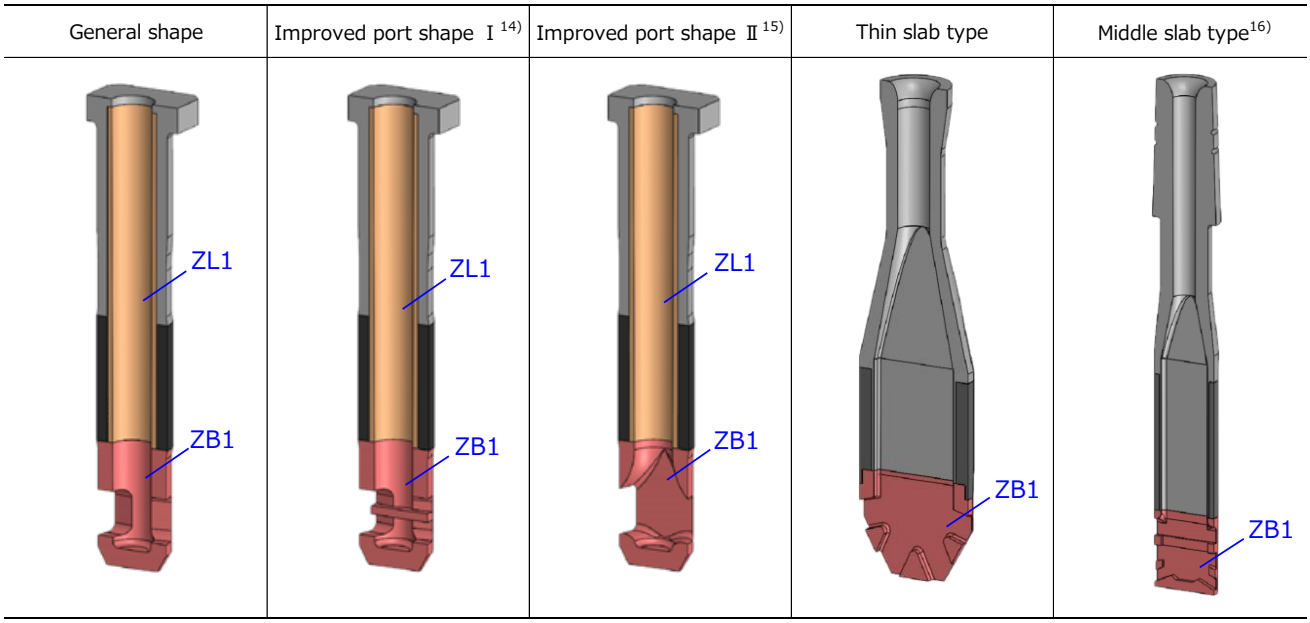

Figure 17. Exemplary design of five types of SEN to which ZL1 and ZB1 are applied.

CONCLUSION

By using ZrO_2-CaO raw material containing free CaO by 40mass% or more with low carbon content, we have succeeded to develop the novel material ZL1 as a high-functional hard-to-adhere property superior to the conventional ZCG and the low erosion in the molten steel flow. The ZL1 was registered as one of the products of the trade mark EVERCLEAN™. The excellent adhesion resistance and high erosion resistance were achieved even in the actual operation by applying the material to the inner wall of the submerged entry nozzle. The improvement of the quality of the steel product was also achieved with the excellent anti-adhesion property obtained by suppressing both the occurrence of the turbulent flow and the entrainment of the mold powder used in the mold. In addition, application of the ZL1 to the high grade steel such as sheet products became feasible. In the near future, contributions to further stable operation and quality improvement in the steel making process have been expected by using the nozzle made of EVERCLEAN™ materials.

REFERENCES

1) R. Tsujino, A. Tanaka, A, Imamura, D. Takahashi and S. Mizoguchi: *Tetsu-to-Hagane*, 80 [10] 31-36 (1994).
2) N. Miyagawa, T. Muroi, Y. Kondo and K. Oguri: *TAIKABUTSU*, 47 [10] 511-512 (1995).
3) S. Koga, J. Amano, K. Morikawa and K. Asano: *TAIKABUTSU*, 57 [2] 84 (2005).
4) E. M. Levin, C. R. Robbins and H. F. McMurdie: Phase Diagrams for Ceramists, Amer. Ceram. Soc. (1964) p105.
5) L. Li, S. Matsumoto, K. Goto and K. Morikawa: *TAIKABUTSU*, 75 [9] 375-381 (2023).
6) L. Li, S. Matsumoto, K. Goto and K. Morikawa: *Krosaki Harima Technical Report*, 170 44-55 (2022).
7) A. Sasaki, K. Morikawa and J. Yoshitomi: *Proc. UNITECR 2011*, 2-A-3 (2011).
8) A. Sasaki, K. Morikawa and J. Yoshitomi: *Proc. 53rd International Colloquium on Refractories, Steel Casting Session*, (Aachen) 199-203 (2010).
9) K. Sasai, Y. Mizukami and H. Yamamura: *Tetsu-to-Hagane*, 79 [9] 55-62 (1993).
10) L. Li and K. Morikawa: *TAIKABUTSU* 70 [10] 492-499 (2018).
11) S. Michelic and C. Bernhard: Steel Res. Int., 93, 2200086 (2022).
12) A. Sasaki, H. Kamio, K. Morikawa, J. Yoshitomi and T. Kayama: *TAIKABUTSU*, 60 [8] 418 (2008).
13) A. Mizobe, T. Yasuda, T. Tsuduki, J. Kurisu and E. Arimitsu: *TAIKABUTSU*, 63 [2] 65-72 (2011).
14) T. Kuroda, A. Mizobe and J. Kurisu: *Krosaki Harima Technical Report*, 158 60-63 (2010).
15) A. Mizobe, K. Tachikawa, J. Kurisu and M. Ueki: *J. Tech. Association of Refractories*, Japan, 38 [1] 35-43 (2018).
16) J. Kurisu, A. Mizobe, H. Furukawa and T. Kuroda: *TAIKABUTSU*, 66 [8] 385-391 (2014).